Melanoma-derived extracellular vesicles mediate lymphatic remodelling and impair tumour immunity in draining lymph nodes

Journal Article

Author(s):
Leary, Noelle; Walser, Sarina; He, Yuliang; Cousin, Nikola; Pereira, Paulo; Gallo, Alessandro; Collado-Diaz, Victor; Halin, Cornelia; Garcia-Silva, Susana; Peinado, Hector; Dieterich, Lothar C.

ISEV

RESEARCH ARTICLE

Melanoma-derived extracellular vesicles mediate lymphatic remodelling and impair tumour immunity in draining lymph nodes

Noelle Leary[1] | Sarina Walser[1] | Yuliang He[1] | Nikola Cousin[1] | Paulo Pereira[1] |
Alessandro Gallo[1] | Victor Collado-Diaz[1] | Cornelia Halin[1] | Susana Garcia-Silva[2] |
Hector Peinado[2] | Lothar C. Dieterich[1]

[1] Institute of Pharmaceutical SciencesSwiss Federal Institute of Technology (ETH) Zurich, Zurich, Switzerland

[2] Microenvironment and Metastasis Laboratory, Spanish National Cancer Research Centre, Madrid, Spain

Correspondence
Lothar C. Dieterich, Institute of Pharmaceutical Sciences, Swiss Federal Institute of Technology (ETH) Zurich, Vladimir-Prelog-Weg 1-5/10, Zurich 8093, Switzerland.
Email: Lothar.Dieterich@pharma.ethz.ch

Abstract

Tumour-draining lymph nodes (LNs) undergo massive remodelling including expansion of the lymphatic sinuses, a process that has been linked to lymphatic metastasis by creation of a pre-metastatic niche. However, the signals leading to these changes have not been completely understood. Here, we found that extracellular vesicles (EVs) derived from melanoma cells are rapidly transported by lymphatic vessels to draining LNs, where they selectively interact with lymphatic endothelial cells (LECs) as well as medullary sinus macrophages. Interestingly, uptake of melanoma EVs by LN-resident LECs was partly dependent on lymphatic VCAM-1 expression, and induced transcriptional changes as well as proliferation of those cells. Furthermore, melanoma EVs shuttled tumour antigens to LN LECs for cross-presentation on MHC-I, resulting in apoptosis induction in antigen-specific CD8$^+$ T cells. In conclusion, our data identify EV-mediated melanoma—LN LEC communication as a new pathway involved in tumour progression and tumour immune inhibition, suggesting that EV uptake or effector mechanisms in LECs might represent a new target for melanoma therapy.

KEYWORDS
exosome, immunotherapy, lymphangiogenesis, pre-metastatic niche, sentinel lymph node

1 | INTRODUCTION

Tumour-draining LNs are essential for tumour progression. They frequently are the first sites of metastasis and have high prognostic value in many cancer types (Karaman & Detmar, 2014; Nathanson et al., 2015). In addition, they have a critical function in the activation of tumour-specific immunity and immunotherapy responsiveness (Dammeijer et al., 2020; Francis et al., 2020). During primary tumour growth, draining LNs frequently undergo massive remodelling, including a marked increase in size and cellularity due to leukocyte influx, but also local proliferation of cells including LN-resident macrophages and stromal cells such as LECs, leading to the expansion of lymphatic sinuses (Dieterich & Detmar, 2016; Stacker et al., 2014). Furthermore, LECs in tumour-draining LNs undergo phenotypic changes. For instance, bulk RNA-sequencing revealed a marked inflammatory response in tumour-draining LN LECs in two independent mouse tumour models, as well as an upregulation of CD41 accompanied by peri-lymphatic fibrin deposition (Commerford et al., 2018). Together, these changes in the draining LNs are believed to contribute to the formation of a 'pre-metastatic niche' (PMN) that facilitates subsequent colonization by tumour cells (Peinado et al., 2017; Sleeman, 2015). Yet, the precise molecular nature of this niche as well as the signals that induce these changes in tumour-draining LNs are still largely unknown.

EVs, lipid membrane-enwrapped subcellular particles with a diameter ranging from ca. 50 nm up to several μms, have emerged as an important component of intercellular tumour-host communication (Becker et al., 2016; Kanada et al., 2016; Tkach & Théry, 2016). EVs are constantly shed by most cells in the body, but their levels are increased in cancer patients (Logozzi et al., 2009). Depending on physical properties such as size or on their origin, EVs have been classified into distinct subcategories such as small and large EVs, 'exosomes' (vesicles derived from endosomal membranes), 'ectosomes' (vesicles derived from the plasma membrane), or apoptotic bodies (Colombo et al., 2014), and recent technological advances allowed for an even more granular EV subset discrimination (Hoshino et al., 2020). However, the nomenclature of EV subsets is inconsistent (Théry et al., 2018; Witwer & Théry, 2019), and strict separation of these distinct EV classes is technically very challenging.

EVs contain various biomolecules derived from their donor cells, including proteins, nucleic acids, or lipids, and can deliver this molecular information over long distances to recipient cells or tissues within the body. Thereby, tumour cell-derived EVs have been described to promote tumour progression in various ways, for instance, inducing tumour cell migration and invasiveness, promoting tumour angiogenesis, and impairing tumour immunity (Kanada et al., 2016; Sheehan & D'souza-Schorey, 2019). Furthermore, tumour-derived EVs released into the blood circulation were shown to regulate systemic metastasis by forming PMNs in distant organs, such as the lung or the liver. In these studies, EV-induced PMN formation was dependent on the education of bone marrow-derived cells, local induction of inflammation and vascular permeability facilitating extravasation of tumour cells (Hoshino et al., 2015; Liu et al., 2016; Peinado et al., 2012). Interestingly, the location of EV-induced PMNs was shown to depend on the presence of specific adhesion molecules (integrins) in tumour-derived EVs that acted as 'homing' receptors directing tumour-derived EVs to their target organs (Hoshino et al., 2015).

While tumour-promoting functions of EVs in the blood circulation have been investigated by a multitude of studies as outlined above, surprisingly little is known about their interactions with the lymphatic system. It is conceivable that tumour cell-derived EVs shed into the surrounding interstitial spaces are primarily drained via tumour-associated lymphatic vessels and are transported to tumour-draining LNs, yet their fate and function within those LNs is largely unknown. About 10 years ago, Hood et al. were the first that observed a rapid accumulation of EVs derived from a murine melanoma cell line (B16F10) in draining popliteal LNs after injecting them into the footpad of mice (Hood et al., 2011). Interestingly, these LNs seemed to act like a retaining filter, as EVs hardly reached downstream LNs. More recently, another study confirmed that interstitially injected tumour cell-derived EVs rapidly entered lymphatic vessels and were transported to draining LNs within a few hours after injection (Srinivasan et al., 2016). Similarly, wound exudate collected after lymphadenectomy in melanoma patients, which is largely composed of lymph, was found to contain high levels of melanoma EVs (Broggi et al., 2019; García-Silva et al., 2019). Together, these studies strongly suggest that a large proportion of EVs released by tumour cells are indeed taken up by lymphatic vessels and are transported to (and possibly retained in) draining LNs. Functionally, injection of melanoma-derived EVs into the footpad was found to facilitate colonization of the popliteal LN by subsequently injected tumour cells, possibly due to the formation of a PMN within the LN by the induction of an inflammatory response (Hood et al., 2011). Similar observations have been made with EVs derived from colorectal cancer cells (Sun et al., 2019). Other studies found that tumour cell-derived EVs were taken up by LN macrophages, in particular CD169^{+} macrophages residing within lymphatic sinuses, which appeared to relay them to B cell follicles (Black et al., 2016; Pucci et al., 2016). Similar to CD169^{+} macrophages, LECs lining the sinuses are also in direct contact with the lymph and have been shown to take up and process lymph-borne antigens (Hirosue et al., 2014). However, conflicting data regarding the capacity of LECs to take up tumour-derived EVs has been published (Broggi et al., 2019; Pucci et al., 2016).

Here, we tracked melanoma-derived EVs, both after interstitial injection as well as after endogenous release, and found a highly selective interaction with a subset of LN macrophages as well as LN LECs. Functionally, EVs induced LN remodelling, reminiscent of the changes observed in tumour-draining LNs, and altered the transcriptional profile of LN LECs, particularly of those lining the floor of the subcapsular sinus. Furthermore, EVs transferred tumour-derived antigens to draining LNs that were subsequently cross-presented by LN LECs, leading to apoptosis of tumour-specific CD8^{+} T cells. Together, our data suggest that tumour—LN communication via EVs contributes to PMN formation and the inhibition of tumour immunity, indicating that therapeutic targeting of EV uptake or effector mechanisms in draining LNs could be beneficial for cancer patients.

2 | MATERIALS AND METHODS

2.1 | Cell lines

B16F10-luc2 cells were purchased from Caliper and maintained in DMEM medium supplemented with Glutamax, pyruvate, and 10% FBS (all Gibco). B16F10-luc2 cells expressing chicken ovalbumin and GFP (B16F10-ova) were generated as described previously (Cousin et al., 2021). In brief, the cells were transduced with a lentiviral vector carrying a pgk promoter-driven full length ovalbumin coding sequence, followed by an internal ribosomal entry site and GFP. After transduction, GFP^{+} cells were FACS-sorted on a FACS Aria II instrument (BD). B16F10-luc2 cells expressing palmitoylated GFP (B16F10-palmGFP) were generated identically, using a lentiviral vector carrying a palmGFP expression cassette (kindly provided by Franz Ricklefs and Xandra Breakefield, Harvard Medical School, USA).

To delete Rab27a expression, the CrispR-Cas9n double nickase approach was used (Ran et al., 2013). In brief, a pair of sgRNAs were designed for a target sequence in the mouse Rab27a gene using the online tool at chopchop.cbu.uib.no and were cloned into pSpCas9(BB)-2 A-GFP (Addgene, 48140). B16F10-ova cells were transfected with the vectors using polyethylenimine. 24 h later, single GFP$^+$ cells were sorted using a FACS ARIA II instrument and expanded in culture. A clone with a deletion of six nucleotides from the Rab27a coding sequence and strongly reduced Rab27a protein expression but unaltered growth kinetics was selected for further use.

HCMel3 cells [(Bald et al., 2014), kindly provided by Dr. Tobias Bald, QIMR Berghofer, Brisbane, Australia] were maintained in RPMI supplemented with 10% FBS, L-Glutamine, non-essential amino acids, 1 mM HEPES (all Gibco) and 20 μM β-mercaptoethanol.

2.2 | Animal studies

C57Bl/6N wildtype mice, Ackr4-GFP reporter mice (Heinzel et al., 2007) and Prox1-CreER^{T2} x Vcam1$^{fl/fl}$ mice (Arasa et al., 2021) were bred inhouse in a SPF facility. Both male and female mice were used in the experiments, in equal ratios between the experimental groups. To induce recombination, Prox1-CreER^{T2} x Vcam1$^{fl/fl}$ mice were treated with 50 mg/kg tamoxifen (Sigma) in sunflower oil for 5 days by intraperitoneal injection. Cre-negative, Vcam1$^{fl/fl}$ littermates served as controls and were equally treated with tamoxifen.

Tumour cell-derived EVs (5 μg) were injected intradermally into the back skin or subcutaneously at the dorsal aspect of the hind paws, with a corresponding dose of liposomes (FormuMax) serving as control where indicated. To detect ovalbumin cross-presentation, a higher EV dose was used (10 μg / injection). In some cases, EVs were co-injected with 5 μg blocking antibodies against VCAM-1 (Dieterich et al., 2019), CD29 (BioXCell BE0232) or CD49d (BioXCell BE0071).

For tumour studies, 200.000 tumour cells were injected intradermally into the back skin, and the tumour growth was monitored using caliper measurements. Mice were sacrificed on day 14 after injection, and the tumour-draining LNs (inguinal + axillary) were collected and processed for flow cytometry.

All animal experiments were approved by the responsible ethics committee (Kantonales Veterinäramt Zürich, license 5/18).

2.3 | EV isolation, labelling and quality control

To isolate mouse melanoma EVs, tumour cells were washed with PBS and cultured for 72 h in their corresponding growth medium with only 1% exosome-free FBS (Gibco). The supernatant was collected, centrifuged at 700 g to pellet debris and cells, filtered through a 450 nm filter, and subsequently concentrated 1000-fold using centrifugal filter units with a 100 kD cutoff to a final volume ≤ 500 μl. Then, EVs were separated from other supernatant constituents using size exclusion chromatography (SEC) using qEV columns (iZON) according to the manufacturer's instructions. The EV-containing fractions (fractions 1–3 after the void volume) were pooled, and the protein content was determined using the BCA assay (Thermo). In some cases, EVs were labelled with DiD (Thermo). To this end, DiD was added to the concentrated supernatant before SEC to a final concentration of 20 μg/ml, and incubated for 5 min. Subsequently, the supernatant was washed twice with PBS before proceeding with the SEC as described. For quality control of the EV-enriched fractions, electron microscopy was performed at the Centre of Optical and Electron Microscopy (ScopeM) of ETH Zurich. In brief, 5 μl of the gently mixed EV dispersion were placed on glow discharged (Emitech K100X) carbon-coated grids (Quantifoil) and were allowed to adsorb for 60 s. Subsequently, the excess liquid was drained with a filter paper and the samples were subjected to negative staining with 2% uranyl acetate by two successive incubations with the staining solution, for 1 s and 15 s, respectively. The grids were air-dried and imaged in a transmission electron microscope (FEI Morgagni 268, Thermo) operated at 100 kV in bright field mode. Size determination by tunable resistive pulse sensing using a qNANO instrument (iZON) was performed according to the manufacturer's instructions.

Human melanoma EVs were isolated and labelled essentially as described previously (García-Silva et al., 2021). In brief, SK-Mel-28 and SK-Mel-147 cells in 150cm^2 flasks (eight flasks / purification) were cultured for 72 h in EV-depleted medium. Supernatant fractions were collected after 72 h and centrifuged at 500 g for 10 min followed by centrifugations at 12000 g for 20 min and 100000 g for 70 min. Finally, the EV pellet was washed with PBS and collected by another ultracentrifugation at 100000 g for 70 min. All centrifugations were performed at 10 °C using a Beckman Optima X100 centrifuge with a Beckman 70.1Ti rotor. EVs were resuspended in PBS and labelled with DiD or PKH26 (Sigma) in 1 ml of PBS for 5 min at RT. Labelled EVs were washed twice in 20 ml of PBS, collected by ultracentrifugation and resuspended in PBS.

2.4 | Western blot

Equal amounts of EVs or total cell lysates were separated on 4–12% bis-Tris gels using MES buffer (Thermo) and transferred to PVDF membranes (Immobilon-P, Millipore). The membrane was blocked in 5% milk in TBS with 0.1% Tween 20, incubated with

primary antibodies (mouse anti-Alix, Cell Signalling 2171; mouse anti-Tsg101, Genetex GTX70255; rabbit anti-ovalbumin, Novus NB600-922-01; rabbit anti-Rab27a, Cell Signalling 69295; mouse anti-b-catenin, Millipore Mab2081), washed, and incubated with corresponding secondary antibodies (sheep anti-mouse-HRP, GE Healthcare NA931 V; goat anti-rabbit-HRP, Dako P0448) before signal development using ECL substrate and ECL Hyperfilm (both GE Healthcare).

2.5 | Proteomic and transcriptomic analysis of EVs

Three independently isolated batches of B16F10-luc2-derived EVs were subjected to complete proteomic profiling using mass spectrometry at the Functional Genomics Centre Zurich (FGCZ). In brief, samples were dried and resuspended in $50 \mu l$ lysis buffer (PreOmics), incubated at $95\,°C$ for 10 min and HIFU-treated for 30 s. Digestion was performed according to the kit instructions (PreOmics). Dried digests were dissolved in $20 \mu l$ 0.1% formic acid, diluted five times, and subjected to LC/MS/MS. Database searches were performed using Mascot. All proteins detectable by at least one unique peptide in at least two of the three replicates were considered present and are listed in Table S1. For transcriptional analysis, complete mRNA was isolated from B16F10-derived EVs and their donor cells using the Nucleospin RNA kit (Macherey-Nagel) according to the manufacturer's instructions (three biological replicates). Library preparation using a miniaturised version of the Smart-seq2 protocol (Picelli et al., 2014) and sequencing with single-read 100 bp chemistry by Illumina NovaSeq 6000 were performed at the FGCZ. Adaptor sequences and low-quality reads were filtered, the resulting reads were subsequently mapped to the mm10 mouse reference genome. RNA alignment metrics on different genomic regions were computed using CollectRnaSeqMetrics from Picard v1.139 (http://broadinstitute.github.io/picard/). Expression counts were generated and differential expression analysis was performed using the DESeq2 package v1.25.5 (Love et al., 2014) using a cut-off of $\log_2$ fold change (FC) ≥ 1 and FDR < 0.05 (Table S2). The entire sequencing data is available at ArrayExpress / accession number E-MTAB-11025.

2.6 | Flow cytometry of EVs

Direct EV cytometry was done using a CytoFLEX S instrument (Beckman Coulter) according to the manufacturer's instructions (Spittler A., Set-up of the CytoFLEX for extracellular vesicle measurement, Application Information Bulletin 2015), using the instrument's violet laser to detect EVs by side scatter. A mix of 100 nm, 200 nm (both iZON) and 500 nm yellow-green beads (Polysciences) were used for EV gating. EVs were diluted in PBS and stained with directly conjugated antibodies (hamster anti-CD29-Fitc, Biolegend 102206; rat anti-CD49d-Fitc, Biolegend 103605; both centrifuged for 10 min at 10.000 g directly before use). Unstained EVs, isotype-stained EVs (hamster IgG-Fitc, Biolegend 400906; rat IgG2bk-Fitc, BD 556923), and antibodies alone were used as controls. Furthermore, a dilution analysis was done to identify potential particle swarming. FACS data was analysed using FlowJo v10 (BD).

2.7 | Flow cytometry of mouse tissues

LNs were collected and processed for flow cytometry as described before (Commerford et al., 2018). The non-stromal fractions obtained after pre-digestion were pooled with one third of the stroma-enriched fraction and used for LN macrophage and T cell analyses. Cell suspensions were resuspended in PBS and treated with anti-CD16/CD32 (clone 93, Biolegend 101302, 1:100) for 20 min on ice before staining. EV uptake by LN stromal cells, macrophages, DCs and lymphocytes was detected using the following antibodies: rat anti-CD31-Fitc (BD 553372) or rat-anti-CD31-APC (BD 551262) or rat anti-CD31-PerCp/Cy5.5 (Biolegend 102522); hamster anti-podoplanin-Pe (eBioscience 12-5381-82) or hamster anti-podoplanin-Pe/Cy7 (eBioscience 25-5381-82); rat anti-CD45-Pe/Cy7 (Biolegend 103113) or rat anti-CD45-PerCp (BD 557235) or rat anti-CD45-APC (eBioscience 17-0451-82); rat anti-CD11b-Fitc (Biolegend 101206) or rat anti-CD11b-PerCp/Cy5.5 (Biolegend 101228) or rat anti-CD11b-BV605 (Biolegend 101257); rat anti-F4/80-biotin (Biorad MCA497BB) followed by streptavidin-Pe (Biolegend 405204) or rat anti-F4/80-Alexa647 (AbD Serotec MCA497A647); rat anti-CD169-Pe/Cy7 (Biolegend 142412); rat anti-MHCII-PerCp (Biolegend 107624) or rat anti-MHCII-Alexa700 (Biolegend 107622); hamster anti-CD11c-Pe/Cy7 (Biolegend 117318) or hamster anti-CD11c-PerCp/Cy5.5 (Biolegend 117328); rat anti-CD8-Fitc (Biolegend 100706) or rat anti-CD8-Apc/Cy7 (Biolegend 100714); rat anti-CD4-Pe (BD 553049); rat anti-B220-Pe/Cy7 (Biolegend 103222). To determine VCAM-1 expression in LN LECs and SIINFEKL cross-presentation, we additionally used the following antibodies: goat anti-VCAM-1 (R&D AF643) followed by donkey anti-goat-Alexa488 or donkey anti-goat-Alexa647 (both Thermo); rat anti-CD45-Apc/Cy7 (Biolegend 103116) or rat anti-CD45-PacificBlue (Biolegend 103126); hamster anti-podoplanin-Pe/Cy7, rat anti-CD44-BV650 (Biolegend 103049); rat anti-Mrc1-Pe (Biolegend 141706); and mouse anti-H2-K^b-SIINFEKL-APC (Biolegend 141606). Ki67 expression was measured using an intracellular FACS staining kit (eBioscience 00-5523-00) with rat anti-Ki67-eFluor450 (eBioscience 58-5698-80). To determine T cell responses in tumour-draining LNs, we additionally used: rat anti-CD45-PacificBlue; hamster anti-CD3-Pe/Cy7

(Biolegend 100320); rat anti-Foxp3-Pe/eFluor610 (Thermo 61-5773-82), rat anti-CD44-BV650, rat anti-CD62L-Alexa700 (Biolegend 104426), rat anti-CD25-BV605 (Biolegend 102035), hamster anti-CD69-Apc/Cy7 (Biolegend 104526), AnnexinV-Apc (Biolegend 640930); and Pe-conjugated tetramers H-2K^b-SIINFEKL; H-2K^b-SVYDFFVWL and H-2D^b-EGSRNQDWL (all from NIH Tetramer Core Facility). Live / dead staining was done using Zombie-Aqua (Biolegend 423102), Zombie-NIR (Biolegend 423106) or 7-AAD (Biolegend 420404). Samples were acquired using a FACS Fortessa (BD), a FACS Aria II (BD) or a CytoFLEX-S instrument (Beckman Coulter) and the data was analysed using FlowJo v10 (BD).

2.8 | Adoptive T cell transfer, isolation of CD8$^+$ T cells and ex vivo functional assays

Naïve CD8$^+$ T cells were isolated from LNs and spleens of Ly5.1$^+$ OT-1 mice using CD8 a microbeads (Miltenyi) according to the manufacturer's instructions and were adoptively transferred into tumour-bearing mice on day 10 after tumour inoculation via the tail vein (1×10^6 in 100 μl RPMI). Effector OT-1 T cells were generated by culturing naïve OT-1 T cells for 72 h in presence of 1 ng/ml SIINFEKL peptide (AnaSpec) and 100 U/ml IL2 (Immunotools).

CD8$^+$ T cells were isolated from tumour-draining axillary and inguinal LNs on day 14 after tumour inoculation. For measuring IFN-γ expression, 300.000 cells / well were cultured for 4 h in presence of GolgiPlug (BD) and stained with Zombie-Aqua, rat anti-CD8-Fitc, rat anti-CD45.1-PerCp (Biolegend 110726) and intracellularly with rat anti-IFN-γ-Pe/Cy7 (Biolegend 505826). To determine proliferation, isolated CD8$^+$ T cells were labelled with CFSE and cultured for 72 h in presence of 200 ng/ml anti-CD3 (Biolegend 100331) and 100 ng/ml anti-CD28 (Biolegend 102112) or in presence of B16F10-ova cells (target:effector ratio 1:5), followed by staining with rat anti-CD8-Apc/Cy7. To determine tumour cell killing, isolated CD8$^+$ T cells were cultured with B16F10-ova cells (target:effector ratio 1:5) for 16 h, followed by staining with Zombie-NIR and rat anti-CD45-PerCp. All data were acquired using a CytoFLEX-S instrument and analysed using FlowJo v10 (BD).

2.9 | Immunofluorescence staining of LN sections and wholemounts

LNs were embedded in O.C.T. compound, snap frozen in liquid nitrogen and stored at -80 °C until preparation of 7 μm-thick cryosections. For staining, sections were first fixed with ice-cold acetone and methanol, then dried and rehydrated in PBS. Subsequently, slides were blocked with blocking solution (PBS with 5% donkey serum, 0.3% Triton-X100, 0.2% BSA, and 0.05% NaN$_3$) before primary antibodies (rabbit anti-Lyve-1, Angiobio 11-034; goat anti-Lyve-1, R&D AF2125; goat anti-Prox1, R&D AF2727; rat anti-Ki67, Dako M7249; rabbit anti-RFP, Rockland 600-401-379; goat anti-VCAM-1, R&D AF643) diluted in blocking solution were applied. After extensive washing, slides were incubated with corresponding secondary antibodies (donkey anti-rat, anti-rabbit, or anti-goat, labelled with Alexa488, Alexa594 or Alexa647, all Thermo) together with Hoechst33342 for nuclear counterstaining, mounted, and imaged using a AxioScop 2 mot plus microscope (Zeiss). For quantification of Ki67$^+$ LECs, microscopic images spanning one entire LN cross section / mouse were analysed by counting the number of Prox1$^+$ nuclei that stained for Ki67 or not using Fiji (Schindelin et al., 2012). For wholemount imaging, LNs were stained and optically cleared as described before (Commerford et al., 2018) and imaged using a light sheet microscope (LaVision).

2.10 | LEC and MSM sorting, scRNA-seq and data analysis

For scRNA-seq, single inguinal LN LECs were sorted into 384-well plates pre-spotted with lysis buffer essentially as described before (Fujimoto et al., 2020), but discarding the cells derived from the first of the three digestion steps. Inguinal LN medullary sinus macrophages (MSMs) were sorted using a mix of negative selection markers in a 'dump' channel (rat anti-CD3-Fitc, Biolegend 100203; rat anti-CD19-Fitc, Biolegend 115505; rat anti-Ly-6G-Fitc, BD 551460) in combination with the positive selection markers rat anti-CD11b-PerCp/Cy5.5, rat anti-CD169-Pe (Biolegend 142403) and rat anti-F4/80-Alexa647.

Library preparation and sequencing by Smart-seq2 was done at the FGCZ as described (Fujimoto et al., 2020). For data analysis, the Nextera adapter sequences and low-quality bases were removed using trimmomatic v0.33 (Bolger et al., 2014). Trimmed reads were aligned to the Ensembl mm10 mouse reference genome (release 92) using STAR v2.4.2 a (Dobin et al., 2013). Gene expression quantification was computed with the 'featureCounts' function in the Rsubread package v1.26.1 (Liao et al., 2019). Quality filtering was performed with the scran package v1.4.5, cells with library size or feature size 2.53 median absolute deviations (MADs) away from the median, or with mitochondrial contents three MADs above the median were dropped as outliers (Lun et al., 2016). For the LN macrophage dataset, cells with less than 500 genes were also removed. Genes expressed in at least 15% of cells were grouped in accordance with their count-depth relationship by SCnorm v0.99.7, which applied a quantile regression within each group to estimate scaling factors and normalize for sequencing depth (Bacher et al., 2017). Cells with detected CD45 expression in the LN LEC dataset were removed before downstream analyses. The top 2000 variable features were identified in the naïve and EV-injected datasets, which were subsequently integrated using the 'FindIntegrationAnchors' and 'IntegrateData'

functions in the Seurat package v3.1.2 (Stuart et al., 2019). Unsupervised clustering was performed on the integrated dataset and visualized with Uniform Manifold Approximation and Projection (UMAP) (Becht et al., 2018). Differentially expressed genes in each respective subtype of cells between naïve and EV-injected conditions were identified by the 'FindMarkers' function (min.pct = 0.20, logfc.threshold = 0.25, p_val_adj < 0.05) using the MAST test (Finak et al., 2015). Expression patterns of selected markers were plotted by the 'FeaturePlot' function. The entire sequencing data is available at ArrayExpress under accession E-MTAB-10434.

2.11 | Analysis of previously published scRNA-seq data of human LN LECs

Raw data were downloaded from GSE124494 and quality control was performed as previously described (Takeda et al., 2019). Briefly, human LN data sets were aligned using Canonical Correlation Analysis (CCA) provided by Seurat v2.3.4, with highly variable genes identified in at least two datasets. Unsupervised clustering was performed using the aligned canonical correlation vectors (CC) 1-30, after which the LEC population was subsetted for downstream analysis (resolution = 0.3). The expression patterns were plotted by the 'VlnPlot' function.

2.12 | Statistical analysis

GraphPad Prism v9 was used to draw graphs and perform statistical tests. Test details are indicated within the individual figure legends.

3 | RESULTS

3.1 | B16F10-derived EVs are transported by lymphatic vessels and are taken up by LN macrophages and LECs

In order to study EV transport by the lymphatic system and their effect on the LN microenvironment, we first established a method to isolate EVs from in vitro cultures of B16F10 melanoma cells using size exclusion chromatography, a method that has been found both efficient and specific for this purpose (Lobb et al., 2015). The resulting EV preparations were highly pure, contained intact EVs with an average diameter between 70 and 130 nm, and were enriched for the classical exosome markers Tsg101 and Alix (Figure S1A-S1C). Proteomic analysis furthermore demonstrated the enrichment of multiple known exosome- and cell adhesion-related proteins, whereas common markers of impure preparations such as albumin or calnexin were not detectable (Figure S1D-S1E, Table S1). In addition, we performed transcriptional characterization of EVs by RNA sequencing. Interestingly, in comparison to their donor cells, B16F10-derived EVs were enriched for intronic sequences (Figure S1F). Nonetheless, differential gene expression analysis identified 6929 genes enriched ($\log_2 FC > 1$, FDR < 0.05) in EVs compared to donor cells, many of which were coding for membrane- and signal transduction-associated proteins (Figure S1G-S1H, Table S2).

To study the fate of these vesicles in vivo, we first isolated EVs from B16F10 cells overexpressing tdTomato in the cytoplasm (Proulx et al., 2013) and injected them subcutaneously into the hind paw. Interestingly, we found widespread tdTomato present in the subcapsular sinus and cortical sinuses of the draining popliteal LN, as early as 2 h after EV injection (Figure 1A). Since we could not completely rule out that tdTomato in draining LNs could be due to small amounts of free or complexes of tdTomato protein co-purified with the EVs, we also used the lipophilic dye DiD to specifically label membrane-surrounded B16F10-derived EVs. In agreement with previous data (Pucci et al., 2016), flow cytometry analysis of popliteal LNs revealed that DiD-labelled B16F10-derived EVs were strongly taken up by CD169^{+} LN macrophages which additionally expressed F4/80, identifying them as medullary sinus macrophages (MSMs) (Gray & Cyster, 2012), whereas CD169^{+} F4/80^{−} subcapsular sinus macrophages (SSMs) and CD169^{−} F4/80^{+} medullary cord macrophages (MCMs) took up relatively few EVs after injection into the hind paw (Figure 1B). Interestingly, and in contrast to the aforementioned report (Pucci et al., 2016), we also found that B16F10-derived EVs were strongly taken up by LN-resident LECs, whereas no uptake was detectable in other stroma cells (blood endothelial cells (BECs), fibroblastic reticular cells (FRCs)), DCs, or lymphocytes (Figure 1C, S2A-S2B). EV uptake by LN MSMs and LECs was largely confined to the primary draining popliteal LN, as only minimal uptake was detectable in secondary LNs (sacral, inguinal) (Figure 1D-1E), confirming that LNs represent an effective barrier for tumour-derived EVs as previously described (Hood et al., 2011). Identical results were obtained using EVs obtained from another C57Bl/6 syngeneic melanoma model (HCMel3) and EVs obtained from the human melanoma cell lines SK-Mel-28 and SK-Mel-147 (Figure S2C-S2E). Furthermore, using recently identified markers to differentiate between LN LEC subsets such as LECs lining the ceiling (cLECs, Ackr4^{+}) and the floor (fLECs, CD44^{+}) of the subcapsular sinus as well those lining medullary sinuses (mLECs, Mrc1^{+}) (Fujimoto et al., 2020), we found that EV uptake was strongest in fLECs and mLECs (Figure 1F, S2F).
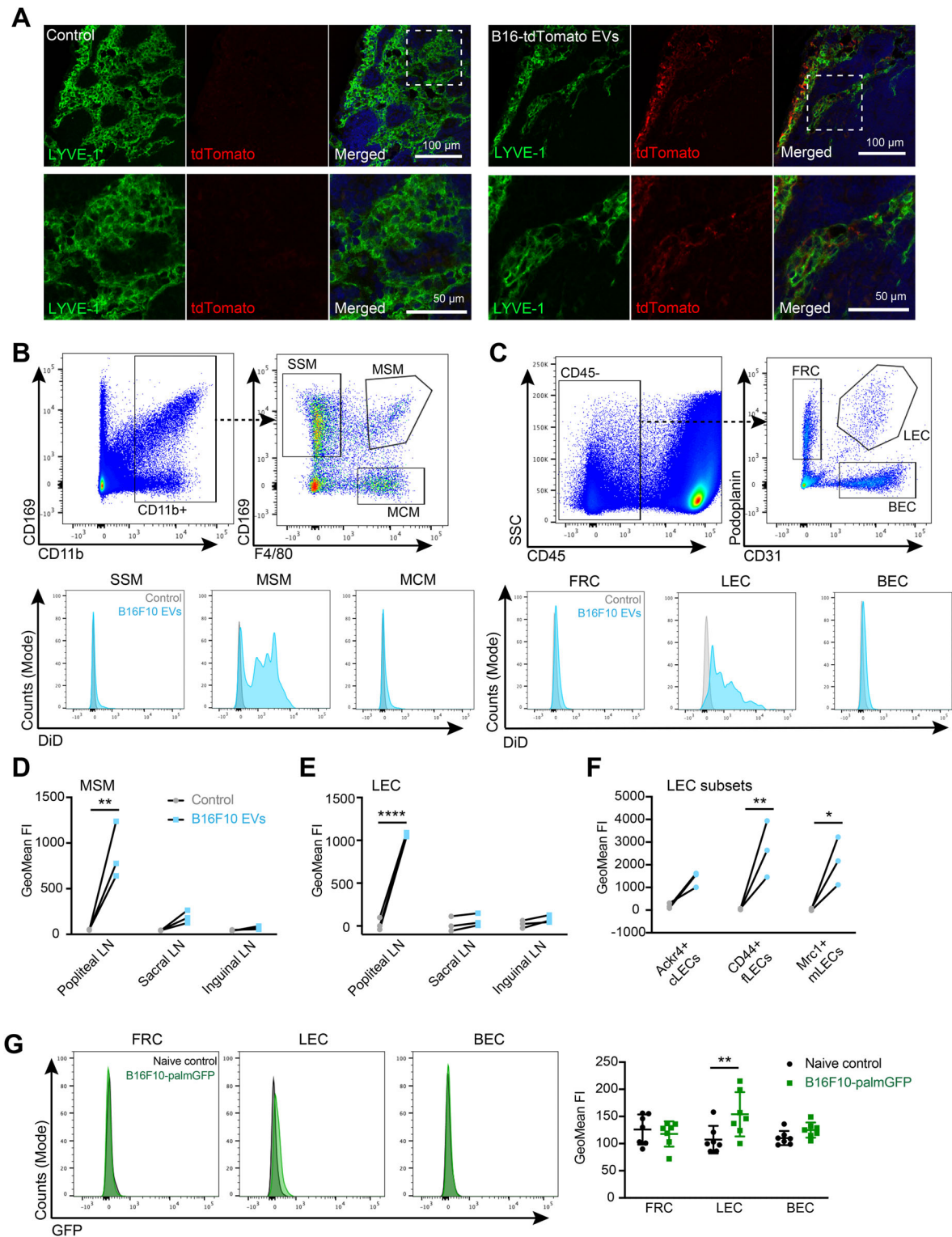
FIGURE 1 B16F10-derived EVs are taken up by LN macrophages and LECs. (A) Microscopic detection of tdTomato in lymphatic sinuses of popliteal LNs 2 h after injection of B16F10-tdTomato-derived EVs into the hind paw. Dashed boxes in the upper panels are shown enlarged in the lower panels. (B) Representative FACS gating for popliteal LN macrophage subsets (SSM, MSM, MCM) (top panels, pre-gated for living singlets) and histograms showing DiD intensity 16 h after injection of B16F10-derived EVs labelled with DiD into the hind paw. (C) Representative FACS gating for popliteal LN stromal cell subsets (FRCs, LECs, BECs) (top panels, pre-gated for living singlets) and histograms showing DiD intensity 16 h after injection of B16F10-derived EVs labelled with DiD into the hind paw. (D, E) Quantification of DiD intensity in MSMs (D) and LECs (E) in popliteal, sacral and inguinal LNs. Each line represents an individual experiment using a pool of 2-3 mice / condition ($N = 3$). (F) Quantification of DiD intensity in LN LEC subsets (ACKR4$^+$ cLECs, CD44$^+$ fLECs, Mrc1$^+$ mLECs). Each line represents an individual experiment using a pool of 2–3 mice / condition ($N = 3$). (G) Representative histograms and quantification of GFP intensity in stromal cells (FRCs, LECs, BECs) of axillary and inguinal LNs draining B16F10 tumours expressing palmitoylated GFP (palmGFP) ($N = 7$ mice / condition). * $p < 0.05$, ** $p < 0.01$, **** $p < 0.0001$, two-way ANOVA with Sidak's post-test (including data matching by experiment in panels D-F)

Bulk injection of in vitro-generated tumour EVs could result in aberrant EV distribution and cellular interactions, compared to a presumably slower but constant 'trickle' of EVs reaching the lymphatic vasculature within or around a growing tumour. To confirm our findings in a model of endogenous melanoma-derived EV release, we generated B16F10 cells expressing membrane-tethered GFP as a tag to follow their EVs (Lai et al., 2015), implanted them intradermally into the back skin of mice, and analysed the tumour-draining LNs (axillary and inguinal) 14 days later. Congruently to our previous data, GFP was slightly but significantly enriched in LN LECs, but not in other stromal cells, DCs, or lymphocytes (Figure 1G, Fig. S2G). In this case, we did not observe GFP in MSMs either (Figure S2G), suggesting that EV uptake by MSMs is either transient, or that MSMs quickly degrade or transfer EV-derived GFP, preventing its accumulation to a detectable level in these cells.

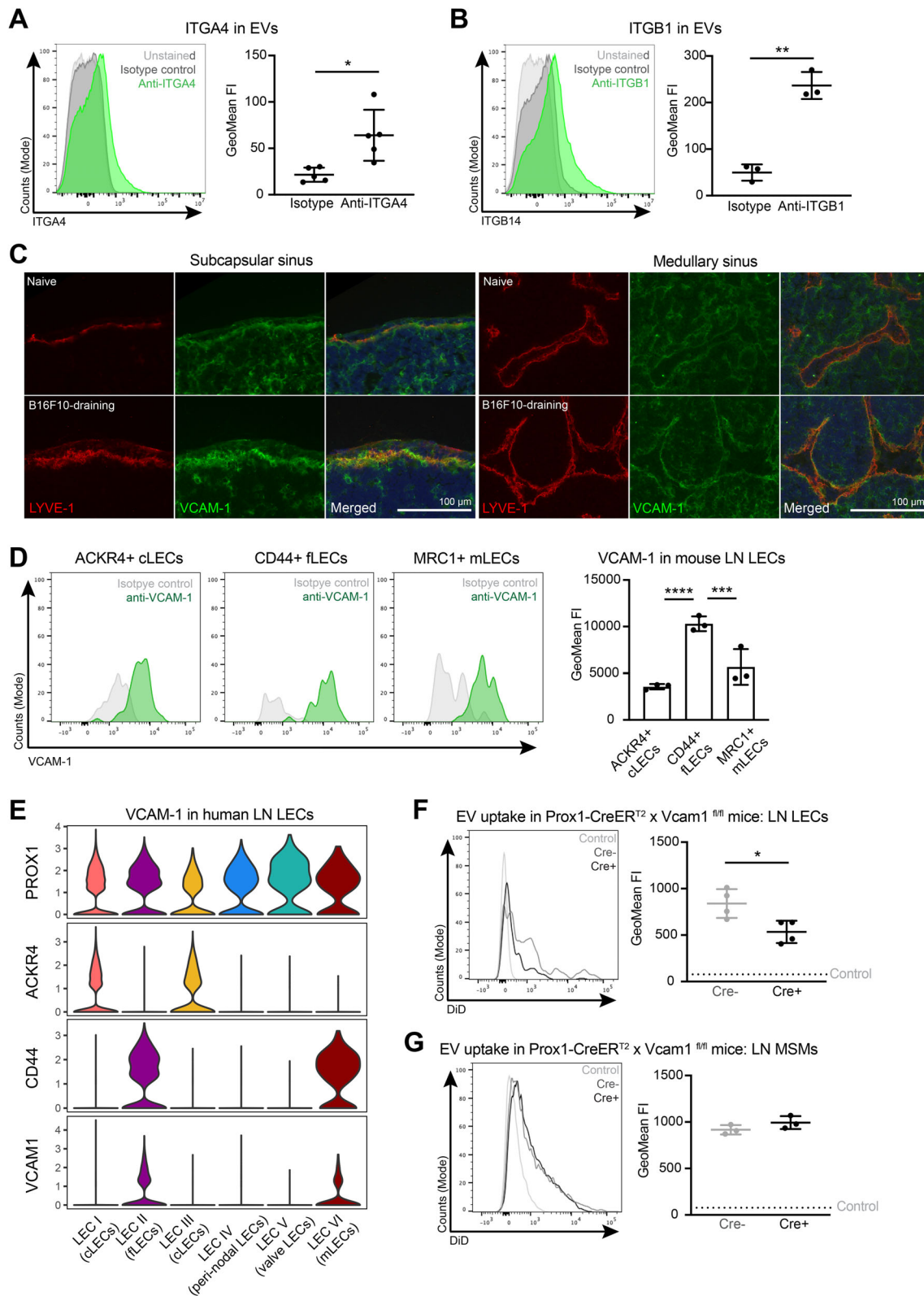## 3.2 | Uptake of B16F10-derived EVs by LN LECs is partially mediated by VCAM-1

The tropism of tumour-derived EVs for specific tissues or recipient cell types has been shown previously to depend on integrins present on the EV surface (Hoshino et al., 2015). We therefore wondered whether integrin-mediated adhesion might also be responsible for the selective uptake of B16F10-derived EVs by LN MSMs and LECs. Interestingly, our proteomic data indicated the presence of multiple integrins in B16F10-derived EVs, including $\alpha 4$, $\alpha 9$ and $\beta 1$ (Table S1), which caught our attention as they form classical receptors for VCAM-1, a cell adhesion protein constitutively expressed by LN LECs and further induced in B16F10 tumour-draining LN LECs (Commerford et al., 2018). Using direct small particle flow cytometry (Figure S3A-S3B), we first validated the presence of $\alpha 4$ (Itga4) and $\beta 1$ (Itgb1) integrins on the surface of B16F10-derived EVs (Figure 2A-2B), while immunofluorescence staining of inguinal LN sections from naive and B16F10-bearing mice confirmed VCAM-1 protein expression in the subcapsular and medullary sinuses (Figure 2C). Furthermore, using flow cytometry we found that VCAM-1 was more highly expressed in fLECs than in cLECs or mLECs (Figure 2D), correlating with EV uptake (Figure 1F). Recently, Takeda et al. performed single-cell RNA sequencing of human LN LECs, identifying six LEC clusters (LEC I-LEC VI) including two types of cLECs, fLECs and mLECs (Takeda et al., 2019). Re-analysing those data, we found that VCAM-1 was also enriched in human fLECs (LEC II) and mLECs (LEC VI) (Figure 2E).

To investigate if VCAM-1 is involved in the uptake of melanoma-derived EVs by LN LECs, we injected labelled EVs into Prox1-CreER^{T2} x Vcam1$^{fl/fl}$ mice that show strongly reduced VCAM-1 expression in LN LECs after tamoxifen treatment (Figure S3C). Indeed, uptake of B16F10- and SK-Mel-28-derived EVs by draining popliteal LN LECs was significantly reduced in these mice, whereas uptake by MSMs was not affected (Figure 2F-2G, S3D-S3E). Congruently, co-injection of EVs together with VCAM-1- or $\beta 1$-neutralizing antibodies decreased EV uptake by LN LECs, but not by MSMs (Figure S3F-S3G). Antibody-mediated blockade of $\alpha 4$ had no measurable effect on EV uptake by LN LECs either (Figure S3F), indicating that $\alpha 9$ present in B16F10-derived EVs might be sufficient to bind LEC-expressed VCAM-1. In conclusion, these data suggest that the uptake of B16F10-derived EVs by LN LECs is partly mediated by integrin—VCAM-1 interactions between EVs and LECs, at least in the setting of acute EV injection.
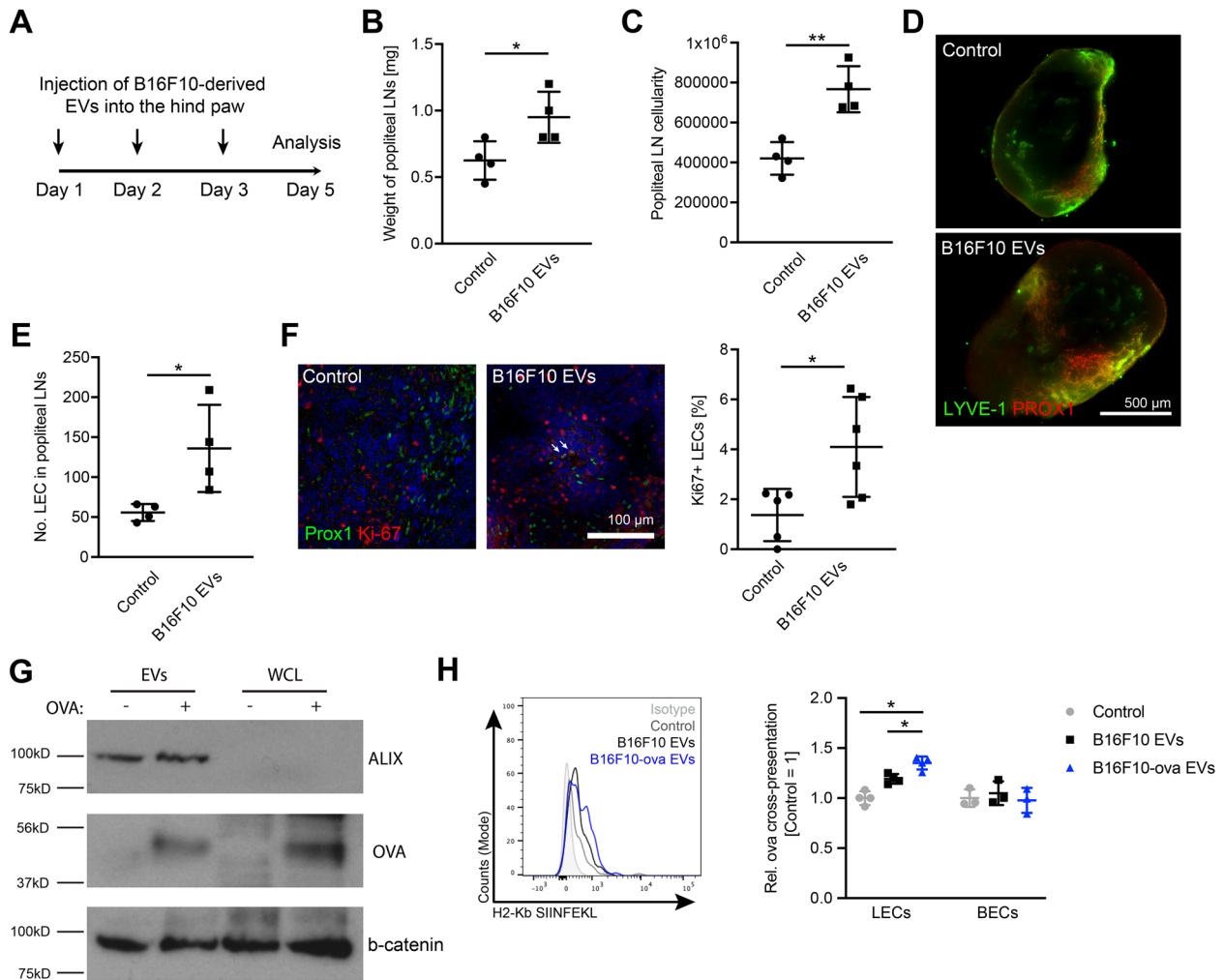
3.3 | B16F10-derived EVs induce lymphatic remodelling and tumour antigen cross-presentation by LECs in draining LNs

To evaluate the acute biologic effects of B16F10-derived EV uptake by LN MSMs and LECs, we treated mice for three consecutive days with EV injections ($5\,\mu g$) into the hind paw as described before, and analysed the draining popliteal LNs 2 days later (Figure 3A). Strikingly, EV injection led to a dramatic increase in the LN weight compared to injection of empty liposomes that were used as control (Figure 3B). This weight increase was not just due to liquid accumulation / edema, as the LN cellularity increased similarly (Figure 3C). Using light-sheet microscopy to take images spanning entire popliteal LNs, we furthermore noted an expansion of Lyve-1$^+$ Prox1$^+$ lymphatic spaces (Figure 3D). Consequently, we found an increased overall number of LN LECs after B16F10 EV injection by flow cytometry (Figure 3E), as well as an increase in the fraction of Ki67$^+$ LECs (Figure 3F), suggesting that B16F10-derived EVs induce LN remodelling and LEC proliferation leading to lymphatic expansion.

Tumour-derived EVs have been suggested to transfer cargo molecules including proteins to recipient cells, although the efficiency of this transfer in vivo is unclear. We therefore wondered if B16F10-derived EVs could transfer potential tumour antigens to LN LECs or MSMs for subsequent processing and presentation to lymphocytes. To investigate this, we engineered B16F10 cells stably expressing chicken ovalbumin (ova) as a model antigen. Ova was readily detectable in EVs as well as whole cell lysates of these cells by western blot (Figure 3G). Notably, injection of B16F10-ova-derived EVs resulted in significant cross-presentation of the ova-derived SIINFEKL peptide on H2-K^b by LN LECs (Figure 3H). In contrast, no SIINFEKL cross-presentation above background was detectable in BECs, MSMs nor any other LN macrophage or DC subset (Figure 3H, S3H).

FIGURE 2 Uptake of B16F10-derived EVs by LN LECs is partly dependent on VCAM-1. (A, B) Representative histogram (left panels) and quantification (right panels) of α4 integrin (ITGA4, A, $N = 5$) and β1 integrin (ITGB1, B, $N = 3$)) on the surface of B16F10-derived EVs detected by small particle flow cytometry. * $p < 0.05$, ** $p < 0.01$, Student's t-test. (C) Representative immunofluorescence images of subcapsular (left) and medullary (right) regions of naïve and B16F10 tumour-draining inguinal LNs stained for Lyve-1 (red) and VCAM-1 (green). (D) Example histograms and quantification of VCAM-1 expression in LN LEC subsets by flow cytometry ($N = 3$). *** $p < 0.001$, **** $p < 0.0001$, one-way ANOVA with Sidak's post-test. (E) Re-analysed single-cell RNA sequencing data of human LN LECs (Takeda et al., 2019) demonstrating enrichment of VCAM-1 transcripts in fLECs (LEC II) and mLECs (LEC IV). (F, G) B16F10-derived EVs labelled with DiD were injected into tamoxifen-treated Prox1-CreER^{T2} x Vcam1$^{fl/fl}$ mice. Example histograms (left panels) and quantification (right panels) of DiD uptake in popliteal LN LECs (F) and MSMs (G) (Control = wildtype mice injected with control liposomes; $N = 3$–4 pools of 2–3 mice each / condition). * $p < 0.05$, unpaired Student's t-test

FIGURE 3 B16F10-derived EVs induce LN remodelling and LEC expansion. (A) Schematic of the experimental workflow to determine acute effects of B16F10-derived EVs on draining LNs. Mice were treated for three consecutive days with 5 µg of B16F10-derived EVs / hind paw, and the popliteal LNs were analysed 2 days after the last injection. (B, C) Weight (B) and total cellularity (C) of popliteal LNs (determined by FACS) ($N = 4$ mice / group). (D) Light sheet microscopy images (maximum intensity projections) of optically cleared LN wholemounts stained for Lyve-1 (green) and Prox1 (red) after injection of control liposomes or B16F10-derived EVs. (E) Total LEC number in popliteal LNs determined by FACS ($N = 4$ mice / group). (F) Representative images and quantification of Ki67^{+} LECs in popliteal LNs ($N = 5$–6 mice / group). Arrows point to Ki67^{+} Prox1^{+} nuclei. * $p < 0.05$, unpaired Student's t-test. (G) Representative western blot of EVs and whole cell lysates (WCL) derived from B16F10 cells with or without ova. (H) Mice were treated with 10 µg EVs derived from B16F10 cells with or without ova / hind paw, and SIINFEKL cross-presentation in popliteal LN LEC and BECs was determined by FACS 1 day later ($N = 3$–4 pools of three mice / condition). Control = mice injected with control liposomes. * $p < 0.05$, two-way ANOVA with Dunnett's post-test

3.4 | B16F10-derived EVs induce long term transcriptional changes in draining LN LECs

To better understand how tumour-derived EVs affect the phenotype of recipient LECs and MSMs in draining LNs in long term, we treated mice with intradermal EV injections into the back skin every other day for a total of 2 weeks, mimicking the usual time span of primary B16F10 tumour growth until reaching the ethically tolerable volume limit of 1 cm³, collected the inguinal LNs, isolated individual LECs by FACS, and performed single-cell RNA sequencing using Smart-seq2 to identify transcriptional changes compared to naïve control mice (Figure 4A). After quality filtering, we analysed a total of 226 naïve and 320 EV-injected LECs, which uniformly expressed CD31 and Prox1, confirming their LEC identity (Figure S4A). These cells clustered into three major subgroups, which we could assign as cLECs, fLECs, and mLECs, based on the specific markers Lyve-1, Ackr4, Madcam1, and Mrc1 (Fujimoto et al., 2020) (Figure 4B, S4A, S4B). In line with our previous findings that EVs interacted strongly with fLECs, differential gene expression ($\log_2$FC > 0.25; $p_{adj} < 0.05$) between naïve and EV-injected LECs showed that the fLEC subset responded most dynamically to the EVs compared to the other subsets. In total, 82 transcripts were significantly upregulated and 143 were downregulated in fLECs after EV injection, whereas only a small number of genes were differentially expressed in cLECs and mLECs (Figure 4C-4D, Table S3). Interestingly, gene ontology analysis of these genes showed a highly significant upregulation of genes associated with the term 'extracellular exosome,' indicating that injected EVs might have transferred mRNAs to recipient
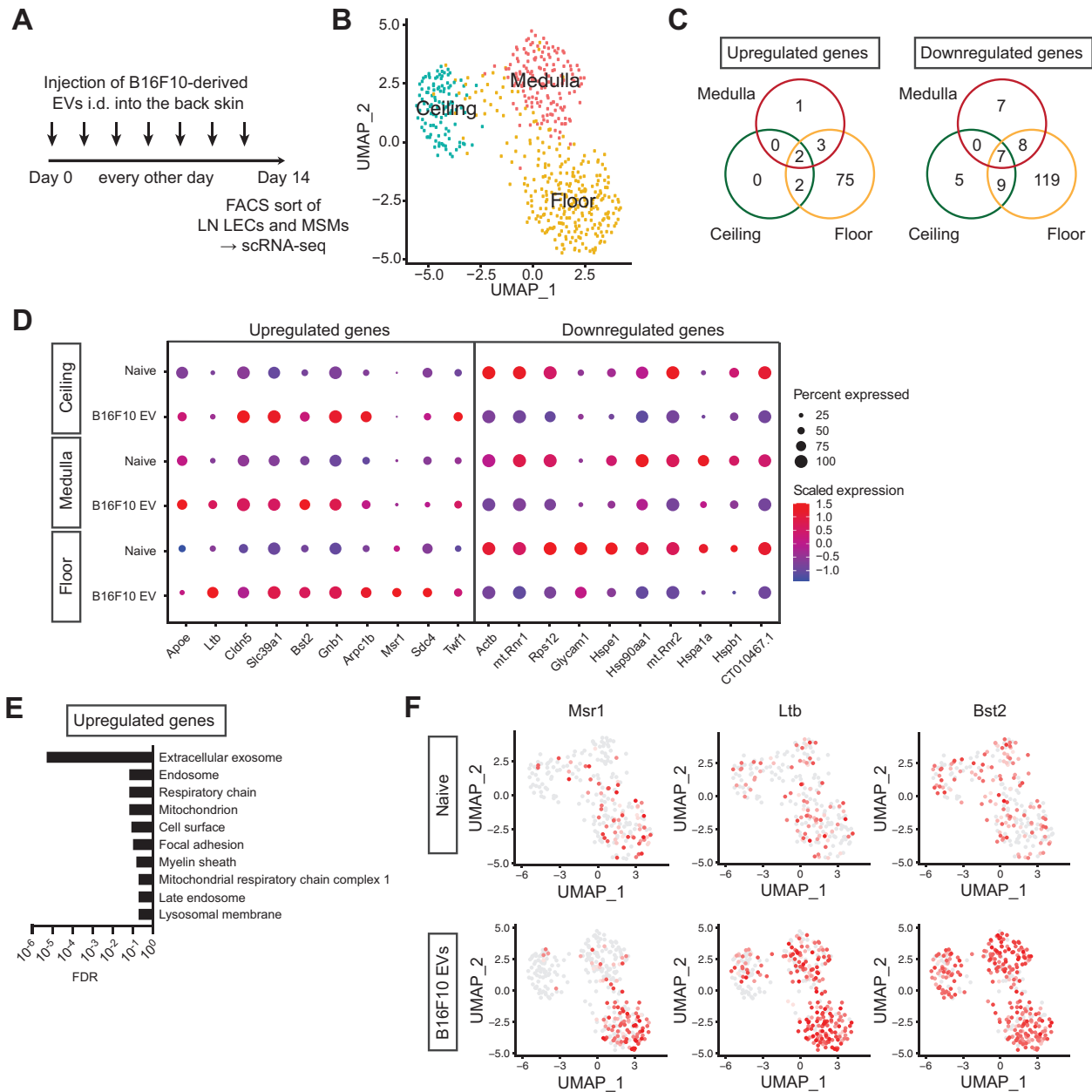
FIGURE 4 B16F10-derived EVs induce transcriptional changes in draining LN LECs. (A) Schematic representation of the experimental approach: Mice were treated every other day by intradermal EV injection for 2 weeks. Subsequently, draining inguinal LNs were collected, LECs isolated and subjected to scRNA-seq. Naïve mice served as controls. (B) Unsupervised clustering of pooled naïve and EV-injected LN LECs and mapping of the three major LN LEC subpopulations: LECs lining the ceiling and the floor of the subcapsular sinus and LECs lining medullary sinuses. (C) Number of differentially expressed genes within the three major subsets. Floor LECs (fLECs) showed by far the highest number of differentially expressed genes. (D) Dot plot representing the top 10 most strongly up- and downregulated genes in fLECs and their expression in all three LEC subsets. (E) Top 10 most significantly (by FDR) enriched gene ontology terms (cellular component and biological process) among the up- and downregulated genes in fLECs. (F) Example plots showing the expression of Msr1, Ltb and Bst2 in naïve (top) and EV-injected (bottom) LN LECs

LECs (Figure 4E). Only one (Gm20489) of the 82 genes upregulated in fLECs was not detectable in EVs (gene counts > 0), whereas six transcripts upregulated by fLECs (Arhgap44, Chst2, Fosl2, Msr1, Ncoa3, Nfib) were also enriched in B16F10-derived EVs compared to their donor cells (Table S2). On the other hand, downregulated genes were enriched in ribosome-associated transcripts (Table S3). The most highly upregulated genes in fLECs in response to EV injection (Figure 4D) included several genes with potential immune regulatory functions, such as macrophage scavenger receptor 1 (Msr1), lymphotoxin-β (Ltb) and bone marrow stromal stromal antigen 2 (Bst2; CD317) (Figure 4E), suggesting that tumour-derived EVs might alter the immune-regulatory capacity of LN LECs. Ltb additionally exerts important functions in LN development (Onder et al., 2013), and might therefore be involved in the tumour-induced LN remodelling and lymphatic expansion.

In addition to LECs, we also FACS-sorted and sequenced MSMs. Surprisingly, although we used stringent gating and negative selection with several lineage markers, gene expression analysis showed that besides macrophages, we had co-isolated various other immune cell types, confirming previous work showing that isolation of pure LN macrophages by FACS is very challenging (Gray et al., 2012). Unsupervised clustering resulted in four major cell subsets, which could be mapped as T cells and NK cells, DCs, and two clusters of macrophages / monocytes that both expressed CD11b (Itgam) and F4/80 (Adgre1) but differed in their expression of, for example, CD209 a, Ly6i, and Clec4a3 (Figure S4C-S4D). Next, we compared the gene expression between naïve LN MSMs and EV-injected MSMs, but found only a handful of genes differentially expressed (eight genes upregulated, 26 genes downregulated, Table S4) in macrophages between the conditions, most of which were similarly regulated between the two clusters of macrophages / monocytes (Figure S4E). This suggests that tumour-derived EVs have more profound effects on the phenotype of recipient LN LECs compared to MSMs.
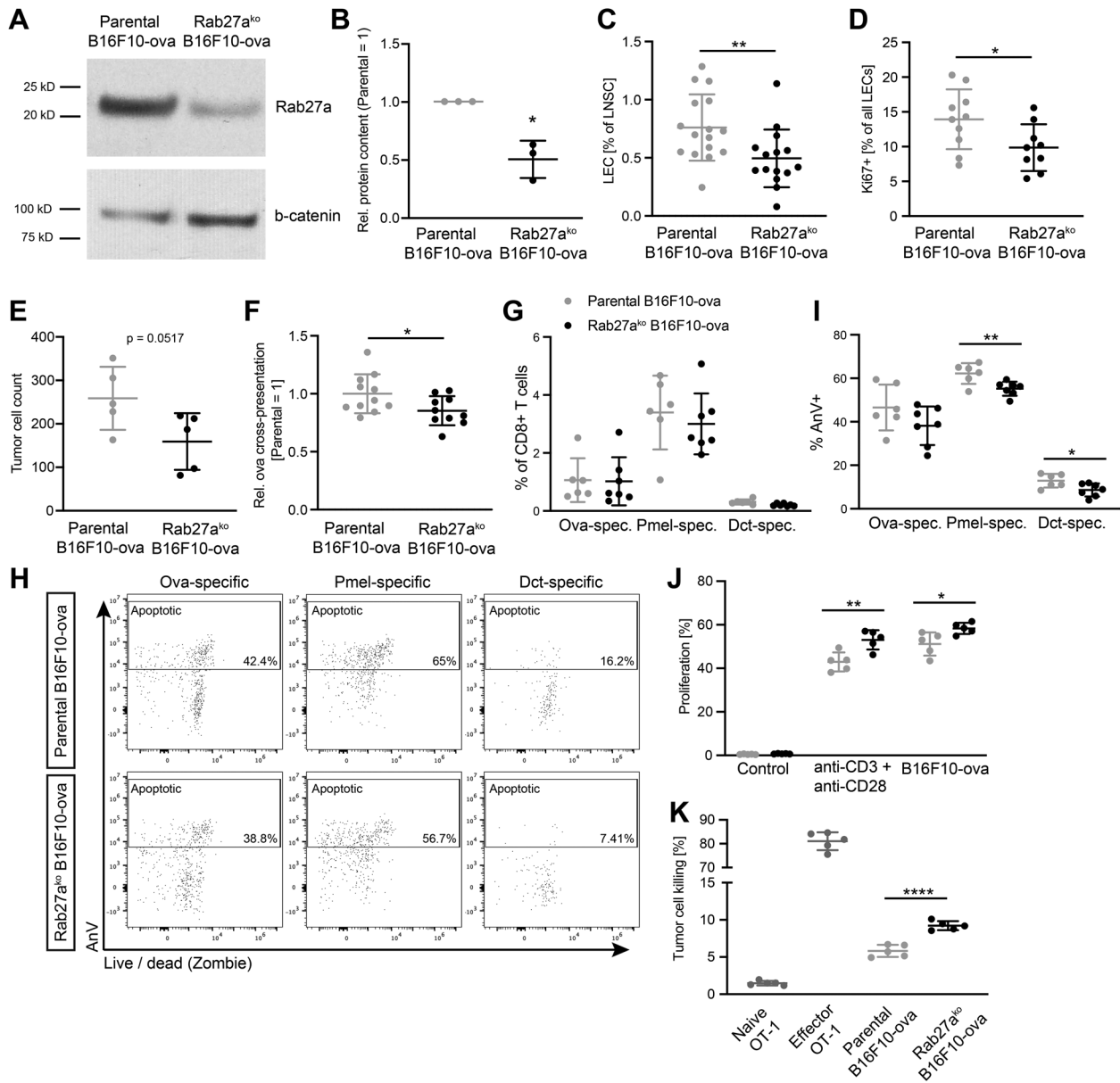
3.5 | Expansion of, and antigen cross-presentation by, tumour-draining LN LECs is reduced in EV release-deficient B16F10 tumours

To confirm that expansion of LN LECs and their cross-presentation of tumour antigens is mediated by EVs not only after EV injection but also in the context of EV release from an endogenous tumour, we next engineered B16F10-ova cells lacking Rab27a, which is required for exosome release (Peinado et al., 2012), using the CrispR-Cas9n double nickase approach. Rab27a^{ko} B16F10-ova cells showed a strongly reduced Rab27a expression in western blot, and their EV release in culture was reduced by roughly 50% (Figure 5A-5B). When implanted into mice, these cells formed tumours as rapidly as parental B16F10-ova cells (Figure S5A), enabling us to compare LEC responses in LNs draining tumours of equal size at the same timepoint. Additional transduction with palmitoylated GFP indicated that EV uptake by LECs was reduced in LNs draining Rab27a^{ko} compared to parental B16F10-ova tumours (Figure S5B). Notably, Rab27a deletion in B16F10-ova cells resulted in a reduced frequency and proliferation (evidenced by Ki67 staining) of LECs and a trend towards reduced numbers of disseminated tumour cells in draining LNs on day 14 after tumour implantation (Figure 5C-5E). In contrast, the frequency and proliferation rate of LN BECs was not altered in LNs draining EV release-deficient tumours (Figure S5C-S5D). Thus, primary tumour-induced lymphatic expansion in draining LNs is at least partly mediated by tumour-derived EVs. In addition, cross-presentation of tumour cell-derived ova by LN LECs was slightly but significantly reduced (Figure 5F), confirming that EVs can shuttle tumour antigen directly to LN LECs which then present them to lymphocytes.

LN LECs have previously been found to present endogenously expressed and scavenged antigen on MHC-I, leading to the inhibition of CD8$^+$ T cells (Cohen et al., 2010; Hirosue et al., 2014; Tewalt et al., 2012). Therefore, we next investigated if reduced EV release from B16F10-ova tumours lacking Rab27a might result in a better anti-tumour T cell response. Using flow cytometry, we found no difference in the frequency of CD3$^+$ T cells in LNs draining B16F10-ova tumours with or without Rab27a (Figure S5E-F). Similarly, neither the frequency of major T cell subsets (CD8$^+$ cytotoxic T cells, CD4$^+$ T helper cells, FoxP3$^+$ Tregs) nor their memory profile or activation (expression of CD25 and CD69) were altered (Figure S5E, S5G-S5I). Recently, we found that LN LECs could inhibit tumour immunity by inducing apoptosis in tumour antigen-specific CD8$^+$ T cells via expression of PD-L1 (Cousin et al., 2021). To investigate whether EV-mediated tumour antigen transfer to LN LECs was involved in this process, we used tetramers in combination with an apoptosis marker (AnnexinV) to detect apoptotic, tumour-specific CD8$^+$ T cells. Interestingly, while the rate of living ova-specific CD8$^+$ T cells was not affected by Rab27a deletion in the primary tumour (Figure 5G), we noted a slight trend towards reduced apoptosis of these cells, whereas CD8$^+$ T cells specific for the endogenous tumour antigens Pmel and Dct (Tyrp2), which are both present in B16F10-derived EVs (Table S1), showed a significant apoptosis reduction in LNs draining Rab27a^{ko} tumours (Figure 5H-5I). To analyse if the functionality of tumour-specific CD8$^+$ T cells in tumour-draining LNs is affected by tumour-derived EVs, we treated mice bearing parental and Rab27a^{ko} B16F10-ova tumours with an adoptive transfer of naïve, ovalbumin-specific CD8$^+$ OT-1 T cells on day 10 after tumour implantation, isolated CD8$^+$ T cells from the draining LNs on day 14, and assessed their functionality ex vivo. Using flow cytometry, we noted that IFN-γ expression was elevated when Rab27a was deleted in the primary tumours, especially in transferred OT-1 T cells (Figure S5 J). More strikingly, proliferation of total CD8$^+$ T cells from LNs draining Rab27a^{ko} was significantly increased, both in response to a low dose of anti-CD3 / anti-CD28 antibodies and to co-culture with B16F10-ova cells (Figure 5J). Likewise, their capacity to kill B16F10-ova cells in vitro was much higher than that of CD8$^+$ T cells derived from LNs draining parental B16F10-ova tumours (Figure 5K). Together, these data show that EV-mediated antigen shuttling from tumour cells to LN LECs has a negative impact on tumour antigen-specific CD8$^+$ T cell responses.

4 | DISCUSSION

Expansion and remodelling of tumour-draining LNs is a well-known phenomenon in both pre-clinical cancer models and cancer patients alike. Interestingly, although LN lymphangiogenesis is considered a hallmark of the LN PMN (Sleeman, 2015), it is still

FIGURE 5 Primary tumour-induced LN LEC expansion and tumour antigen cross-presentation are mediated by EVs. (A) Representative western blot of Rab27a in whole cell lysates of parental B16F10-ova cells and B16F10-ova cells deficient of Rab27a. (B) EV release of parental B16F10-ova cells and Rab27a[ko] B16F10-ova cells in vitro quantified by protein content of isolated EVs ($N = 3$). * $p < 0.05$, one-sample t-test. (C-D) Mice were challenged with parental B16F10-ova cells or Rab27a[ko] B16F10-ova cells and the draining axillary and inguinal LNs were analysed on day 14 after tumour cell injection by flow cytometry. Frequency of LECs among all stroma cells (C, $N = 15–16$ mice / condition, pooled from three independent experiments) and frequency of Ki67^{+} LECs (D, $N = 9–10$ mice / condition, pooled from two independent experiments). (E) Number of CD45^{−} CD31^{−} GFP^{+} tumour cells in LNs draining parental B16F10-ova or Rab27a[ko] B16F10-ova tumours additionally expressing palmGFP ($N = 5$ mice / condition). (F) SIINFEKL cross-presentation by LECs in LNs draining parental B16F10-ova or Rab27a[ko] B16F10-ova tumours expressed as normalized geometric mean intensity values ($N = 10–11$ mice / condition, pooled from two individual experiments). (G) Frequency of T cells specific for ovalbumin, Pmel (gp100) and Dct (Tyrp2) among all CD8^{+} T cells in LNs draining parental B16F10-ova (grey) and Rab27a-deficient B16F10-ova tumours (black) ($N = 6–7$ mice / condition). (H-I) Representative FACS plots (H) and rate of apoptosis determined by AnnexinV (AnV) staining (I) among CD8^{+} T cells specific for ovalbumin, Pmel (gp100) and Dct (Tyrp2) in LNs draining parental B16F10-ova (grey) and Rab27a-deficient B16F10-ova tumours (black) ($N = 6–7$ mice / condition). (J-K) CD8^{+} T cells were isolated on day 14 from tumor-draining LNs of mice bearing parental B16F10-ova or Rab27a[ko] B16F10-ova tumours that were treated with an adoptive transfer of naïve OT-1 T cells on day 10. Proliferation (assessed by CFSE dilution) was determined after 72 h in presence of anti-CD3 / anti-CD28 antibodies or of B16F10-ova cells (J), and the capacity to kill B16F10-ova target cells was determined after 16 h (K). Naïve and ex vivo stimulated effector OT-1 T cells served as negative and positive controls ($N = 5$ / condition). * $p < 0.05$, ** $p < 0.01$, **** $p < 0.0001$, unpaired Student's t-test

not entirely clear how exactly LN lymphangiogenesis facilitates LN metastasis. Previous work suggested that cytokines and growth factors, including VEGF-C and VEGF-A that may be derived from the tumour microenvironment and reach draining LNs via afferent lymph but may also be produced locally, contribute the formation of the LN PMN (Hirakawa et al., 2007; Hirakawa et al., 2005). Here we have identified tumour cell-derived EVs as an additional mediator of tumour-to-LN communication that may be particularly relevant for phenotypic and structural changes in tumour-draining LN LECs.

Our observation that melanoma-derived EVs interact with CD169^{+} macrophages in draining LNs is in line with previous reports (Black et al., 2016; Pucci et al., 2016). However, in contrast to a previous study by Pucci et al. (Pucci et al., 2016), we also found a significant EV uptake by LN LECs. This uptake pattern is consistent with very recent findings by Garcia-Silva et al. (García-Silva et al., 2021). The discrepancy between these finding may be due to the fact that Pucci et al. used a cell surface protein present in their EVs to identify recipient cells. This implies that cells which rapidly internalized EVs and store or degrade their contents may have been missed using this approach. Furthermore, LN LECs comprise a very minor cell population in LNs compared to myeloid or lymphoid cells, and appropriate tissue digestion protocols are necessary to detect them in meaningful numbers by flow cytometry.

Work by David Lyden's group has shown that the interaction of tumour EVs with recipient cells after systemic injection depends on EV integrins (Hoshino et al., 2015). In line with this, we found that B16F10 melanoma-derived EV uptake by LN LECs was partially mediated by lymphatic VCAM-1, which presumably serves as adhesion receptor for EV integrins such as $\alpha4\beta1$ (VLA-4) or $\alpha9\beta1$. On the other hand, other uptake mechanisms and receptors must be involved as well, for instance other integrins such as αV (García-Silva et al., 2021) or scavenger receptors such as Msr1 or Mrc1 that are expressed by fLECs and mLECs (Fujimoto et al., 2020) which most vigorously took up tumour EVs. Also, Bst2, which we found to be upregulated in fLECs and mLECs after EV injection, has been reported to mediate cellular interactions with EVs (Edgar et al., 2016). Furthermore, although MSMs also express VCAM-1 (Tacconi et al., 2021), antibody-mediated VCAM-1 blockade had no effect on their capacity to take up EVs. Additionally, although MSMs readily acquired DiD after EV injection, they did not accumulate sufficient endogenously released palmGFP-tagged EVs to reach the detection limit. This suggests that MSMs interact with EVs in a very different way than LN LECs. While the latter appear to accumulate EVs and process their contents for antigen presentation (in line with the reported antigen archive capacity in the context of virus infections (Tamburini et al., 2014)), MSMs might either quickly degrade or pass EVs (or their constituents) on to other cell types, such as FDCs. In line with the latter hypothesis, LN sinus macrophages have been reported to be poorly phagocytic, but to instead transfer captured particles or antigens into B cell follicles (Phan et al., 2009).

Notably, human melanoma cell-line derived EVs showed a very similar pattern of interaction with LN MSMs and LECs after injection, the latter at least partially mediated by lymphatic VCAM-1 (Figure S2D-E and S3D-E). In line with this, $\alpha4$ and $\beta1$ integrins are present and enriched in EVs derived from human melanoma cells as compared to normal melanocyte-derived EVs (García-Silva et al., 2019). $\alpha4$ and / or $\beta1$ integrins were also detected in melanoma EVs isolated from wound exudate collected after lymphadenectomy in melanoma patients (Broggi et al., 2019; García-Silva et al., 2019) and were enriched in plasma-derived melanoma EVs compared to non-melanoma EVs (Sharma et al., 2020). At the same time, human LN LECs express VCAM-1, particularly fLECs and mLECs, similar to what we observed in mice (Figure 2C-E). Furthermore, melanoma cell expression of $\alpha4\beta1$ integrin has been found to correlate with short disease-free and overall survival of melanoma patients (Schadendorf et al., 1993; Schadendorf et al., 1995). Together, these data suggest that similar molecular interactions might occur between melanoma-derived EVs and LN LECs in melanoma patients, and that these interactions contribute to tumour progression.

Upon uptake by LN LECs, B16F10-derived EVs induced long term changes in gene expression, particularly in fLECs lining the floor of the subcapsular sinus. However, many of these changes could also be observed in mLECs and even cLECs (Figure 4D), although they did not reach statistical significance on those LEC subsets. This is in line with the pattern of EV uptake, which was stronger in fLECs and mLECs than in cLECs. Curiously, many of the differentially expressed genes we identified have been associated with exosomes before, and almost all of them were detectable in isolated, B16F10-derived EVs, suggesting that these EVs were capable of horizontal mRNA transfer to their recipient cells, at least under our experimental conditions. However, our sequencing data is not a proof that these mRNAs were complete and functional, and we cannot exclude that EVs may have induced de novo expression of some of these genes by LN LECs. In addition to EV-associated transcripts, we noted the upregulation of several genes involved in the regulation of immunity and inflammation, including Ltb, a cytokine that is known to regulate not only the development, but also the pathology-associated remodelling of LN stroma, including LN vasculature (Lu & Browning, 2014; Zhu & Fu, 2011). Thus, it is tempting to speculate that EV-induced Ltb in LN LECs may be involved in the expansion of the lymphatic endothelium, but further studies are needed to confirm this hypothesis. Recently, it was shown melanoma-derived EVs transfer NGFR protein to LECs in draining LNs, promote LN metastasis, and trigger MAPK and NF$_k$B signalling and lymphangiogenic gene expression in cultured human LECs after acute EV treatment in vitro (García-Silva et al., 2021). The fact that we did not observe such a striking lymphangiogenesis-associated gene expression profile in LN LECs after 2 weeks of EV treatment suggests that expression of these genes may be acute and transient, depend on the species, and / or the in vitro vs. in vivo environment. In addition, since in our hands B16F10 tumours implanted intradermally into the back skin of mice rarely progress to form overt LN metastasis, we could not confirm that EV-mediated LN lymphangiogenesis contributes to PMN formation and LN metastasis. On the other hand, reduced numbers of single, disseminated tumour cells in LNs draining Rab27a-deficient tumours suggest that EVs indeed promote seeding and / or survival of these cells in the LN microenvironment.

During the last decade, LN LECs have emerged as significant regulators of adaptive T cell immunity, maintaining peripheral tolerance and restricting tumour immunity by antigen presentation on MHC-I and MHC-II and concomitant expression of T cell inhibitory molecules such as PD-L1, which we recently found to induce apoptosis of tumour antigen-specific $CD8^+$ T cells (Cohen et al., 2010; Cousin et al., 2021; Hirosue et al., 2014; Tewalt et al., 2012). Thus, tumour antigen transfer to LN LECs via EVs and subsequent cross-presentation on MHC-I likely inhibits tumour immunity, although we cannot exclude that EVs additionally affect lymphocytes in draining LNs directly. For instance, whereas we and others (García-Silva et al., 2021) found that lymphocytes do not themselves take up melanoma-derived EVs (Figure S2B), immune-regulatory molecules present on the EV surface might still have triggered inhibitory signals in lymphocytes upon direct contact. One limitation of our study is that the effects of Rab27a deletion in the primary tumour on ova presentation by LN LECs and on ova-specific $CD8^+$ T cell apoptosis were not very prominent. Most likely, this was due to several reasons. Firstly, Rab27a deletion reduced the EV release by B16F10-ova cells only by about 50%, suggesting that there were still considerable numbers of tumour-derived EVs reaching the draining LNs over the 2-week period of tumour growth. Secondly, tumour cells ectopically expressing ova presumably secrete free protein into the interstitial fluid, which could therefore reach the draining LNs independently of EVs and might be taken up by LN LECs directly as described previously (Hirosue et al., 2014). Conceivably, shuttling of intracellular tumour antigens that are not usually secreted, such as Pmel or Dct, to LN LECs should depend more strictly on EVs, and indeed, Rab27a deletion had a more pronounced effect on apoptosis induction of $CD8^+$ T cells specific for those antigens. Finally, the B16F10 melanoma model is known to be poorly immunogenic, and generally elicits very weak T cell responses by the host. Therefore, further studies are needed to investigate if EV-mediated tumour antigen transfer to LN LECs has stronger effects on $CD8^+$ T cell responses in more immunogenic tumour models and / or in the context of immunotherapy.

In conclusion, our data demonstrate that melanoma-derived EVs contribute to the relay of molecular information to recipient cells such as LECs in tumour-draining LNs, and are causally involved in pathological LN remodelling and immune inhibition. Consequently, molecules involved in the interaction between EVs and their recipient cells or in their biological functions, such as VCAM-1 and Ltb, may represent new therapeutic targets to restrain tumour progression.

AUTHOR CONTRIBUTIONS
Noelle Leary: Investigation; Methodology. Sarina Walser: Data curation; Formal analysis; Investigation. Yuliang He: Data curation; Formal analysis; Software; Visualization; Writing–review & editing. Nikola Cousin: Investigation. Paulo Pereira: Formal analysis; Investigation. Alessandro Gallo: Formal analysis; Investigation. Victor Collado-Diaz: Resources. Cornelia Halin: Resources; Writing–review & editing. Hector Peinado: Resources; Writing–review & editing

CONFLICT OF INTEREST
The authors declare no conflict of interest.

REFERENCES
Arasa, J., Collado-Diaz, V., Kritikos, I., Medina-Sanchez, J. D., Friess, M. C., Sigmund, E. C., Schineis, P., Hunter, M. C., Tacconi, C., Paterson, N., Nagasawa, T., Kiefer, F., Makinen, T., Detmar, M., Moser, M., Lämmermann, T., & Halin, C. (2021). Upregulation of VCAM-1 in lymphatic collectors supports dendritic cell entry and rapid migration to lymph nodes in inflammation. *Journal of Experimental Medicine*; *218*(7).

Bacher, R., Chu, Li-F., Leng, N., Gasch, A. P., Thomson, J. A., Stewart, R. M., Newton, M., & Kendziorski, C. (2017). SCnorm: Robust normalization of single-cell RNA-seq data. *Nature Methods*; *14*(6), 584–586.

Bald, T., Landsberg, J., Lopez-Ramos, D., Renn, M., Glodde, N., Jansen, P., Gaffal, E., Steitz, J., Tolba, R., Kalinke, U., Limmer, A., Jönsson, G., Hölzel, M., & Tüting, T. (2014). Immune cell–Poor melanomas benefit from PD-1 blockade after targeted type I IFN activation. *Cancer Discovery*; *4*(6), 674–687.

Becht, E., McInnes, L., Healy, J., Dutertre, C. A., Kwok, I. W. H., & Ng, L. G. et al. (2018) Dimensionality reduction for visualizing single-cell data using UMAP. *Nature Biotechnology*.

Becker, A., Thakur, B. K., Weiss, J. M., Kim, H. S., Peinado, H., & Lyden, D. (2016). Extracellular vesicles in cancer: Cell-to-cell mediators of metastasis. *Cancer Cell*.;*30*(6), 836–848.

Black, L. Vc, Saunderson, S. C., Coutinho, F. P., Muhsin-Sharafaldine, M. R., Damani, T. T., Dunn, A. C., & Mclellan, A. D. (2016). The CD169 sialoadhesin molecule mediates cytotoxic T-cell responses to tumour apoptotic vesicles. *Immunology and Cell Biology*; *94*(5), 430–438.

Bolger, A. M., Lohse, M., & Usadel, B. (2014). Trimmomatic: A flexible trimmer for Illumina sequence data. *Bioinformatics* ; *30*(15), 2114–2120.

Broggi, M. A. S., Maillat, L., Clement, C. C., Bordry, N., Corthésy, P., Auger, A., Matter, M., Hamelin, R., Potin, L., Demurtas, D., Romano, E., Harari, A., Speiser, D. E., Santambrogio, L., & Swartz, M. A. (2019). Tumor-associated factors are enriched in lymphatic exudate compared to plasma in metastatic melanoma patients. *Journal of Experimental Medicine*, 1091–1107.

Cohen, J. N., Guidi, C. J., Tewalt, E. F., Qiao, H., Rouhani, S. J., Ruddell, A., Farr, A. G., Tung, K. S., Engelhard, V. H. (2010) Lymph node-resident lymphatic endothelial cells mediate peripheral tolerance via Aire-independent direct antigen presentation. *Journal of Experimental Medicine*; *207*(4), 681–688.

Colombo, M., Raposo, G., & Théry, C. (2014). Biogenesis, secretion, and intercellular interactions of exosomes and other extracellular vesicles. *Annual Review of Cell and Developmental Biology*; *30*, 255–289.

Commerford, C. D., Dieterich, L. C., He, Y., Hell, T., Montoya-Zegarra, J. A., Noerrelykke, S. F., Russo, E., Röcken, M., & Detmar, M. (2018). Mechanisms of tumor-induced lymphovascular niche formation in draining lymph nodes. *Cell reports*; *25*(13), 3554.e4–3563.e4.

Cousin, N., Cap, S., Dihr, M., Tacconi, C., Detmar, M., & Dieterich, L. C. (2021). Lymphatic PD-L1 expression restricts tumor-specific CD8+ T cell responses. *Cancer Research*; *81*(15), 4133–4144,

Dammeijer, F., Van Gulijk, M., Mulder, E. E., Lukkes, M., Klaase, L., Van Den Bosch, T., Van Nimwegen, M., Lau, S. P., Latupeirissa, K., Schetters, S., Van Kooyk, Y., Boon, L., Moyaart, A., Mueller, Y. M., Katsikis, P. D., Eggermont, A. M., Vroman, H., Stadhouders, R., Hendriks, R. W.…Aerts, J. G. (2020). The PD-1/PD-L1-checkpoint restrains T cell immunity in tumor-draining lymph nodes. *Cancer Cell*; *38*(5), 685.e8–700.e8.

Dieterich, L. C., & Detmar, M. (2016). Tumor lymphangiogenesis and new drug development. *Advanced Drug Delivery Reviews*; *99*(Pt B), 148–160.

Dieterich, L. C., Kapaklikaya, K., Cetintas, T., Proulx, S. T., Commerford, C. D., Ikenberg, K., Bachmann, S. B., Scholl, J., & Detmar, M. (2019). Transcriptional profiling of breast cancer-associated lymphatic vessels reveals VCAM-1 as regulator of lymphatic invasion and permeability. *International Journal of Cancer*; *145*(10), 2804–2815.

Dobin, A., Davis, C. A., Schlesinger, F., Drenkow, J., Zaleski, C., Jha, S., Batut, P., Chaisson, M., & Gingeras, T. R. (2013). STAR: Ultrafast universal RNA-seq aligner. *Bioinformatics*; *29*(1), 15–21.

Edgar, J. R., Manna, P. T., Nishimura, S., Banting, G., & Robinson, M. S. (2016). *Tetherin is an exosomal tether. Elife*; *5*.

Finak, G., Mcdavid, A., Yajima, M., Deng, J., Gersuk, V., Shalek, A. K., Slichter, C. K., Miller, H. W., Mcelrath, M. J., Prlic, M., Linsley, P. S., & Gottardo, R. (2015). MAST: A flexible statistical framework for assessing transcriptional changes and characterizing heterogeneity in single-cell RNA sequencing data. *Genome Biology*; *16*, 278.

Francis, D. M., Manspeaker, M. P., Schudel, A., Sestito, L F., O'melia, M. J., Kissick, H. T., Pollack, B, P., Waller, E K., Thomas, S. N. (2020) Blockade of immune checkpoints in lymph nodes through locoregional delivery augments cancer immunotherapy. *Science Translational Medicine*; *12*(563).

Fujimoto, N., He, Y., D'addio, M., Tacconi, C., Detmar, M., & Dieterich, L. C. (2020). Single-cell mapping reveals new markers and functions of lymphatic endothelial cells in lymph nodes. *Plos Biology*; *18*(4), e3000704.

García-Silva, S., Benito-Martín, A., Nogués, L., Hernández-Barranco, A., Mazariegos, M. S., Santos, V., Hergueta-Redondo, M., Ximénez-Embún, P., Kataru, R. P., Lopez, A. A., Merino, C., Sánchez-Redondo, S., Graña-Castro, O., Matei, I., Nicolás-Avila, J. Á., Torres-Ruiz, R., Rodríguez-Perales, S., Martínez, L., Pérez-Martínez, M.…Peinado, H. (2021). Melanoma-derived small extracellular vesicles induce lymphangiogenesis and metastasis through an NGFR-dependent mechanism. *Natural Cancer*; *2*(12), 1387–1405.

García-Silva, S., Benito-Martín, A., Sánchez-Redondo, S., Hernández-Barranco, A., Ximénez-Embún, P., Nogués, L., Mazariegos, M. S., Brinkmann, K., Amor López, A., Meyer, L., Rodríguez, C., García-Martín, C., Boskovic, J., Letón, R., Montero, C., Robledo, M., Santambrogio, L., Sue Brady, M., Szumera-Ciećkiewicz, A.…Peinado, H. (2019). Use of extracellular vesicles from lymphatic drainage as surrogate markers of melanoma progression and BRAF (V600E) mutation. *Journal of Experimental Medicine*; *216*(5), 1061–1070.

Gray, E. E., & Cyster, J. G. (2012). Lymph node macrophages. *Journal of Innate Immunity*; *4*(5-6), 424–436.

Gray, E. E., Friend, S., Suzuki, K., Phan, T. G., & Cyster, J. G. (2012). Subcapsular sinus macrophage fragmentation and CD169+ bleb acquisition by closely associated IL-17-committed innate-like lymphocytes. *Plos One*; *7*(6), e38258.

Heinzel, K., Benz, C., & Bleul, C. C. (2007). A silent chemokine receptor regulates steady-state leukocyte homing in vivo. *Proceedings of the National Academy of Sciences of the United States of America*; *104*(20), 8421–8426.

Hirakawa, S., Brown, L. F., Kodama, S., Paavonen, K., Alitalo, K., & Detmar, M. (2007). VEGF-C-induced lymphangiogenesis in sentinel lymph nodes promotes tumor metastasis to distant sites. *Blood*; *109*(3), 1010–1017.

Hirakawa, S., Kodama, S., Kunstfeld, R., Kajiya, K., Brown, L. F., & Detmar, M. (2005). VEGF-A induces tumor and sentinel lymph node lymphangiogenesis and promotes lymphatic metastasis. *Journal of Experimental Medicine*; *201*(7), 1089–1099.

Hirosue, S., Vokali, E., Raghavan, V. R., Rincon-Restrepo, M., Lund, A. W., Corthésy-Henrioud, P., Capotosti, F., Halin Winter, C., Hugues, S., & Swartz, M. A. (2014). Steady-state antigen scavenging, cross-presentation, and CD8+ T cell priming: A new role for lymphatic endothelial cells. *Journal of Immunology*; *192*(11), 5002–5011.

Hood, J. L., San, R. S., & Wickline, S. A. (2011). Exosomes released by melanoma cells prepare sentinel lymph nodes for tumor metastasis. *Cancer Research*; *71*(11), 3792–3801.

Hoshino, A., Costa-Silva, B., Shen, T. L., Rodrigues, G., Hashimoto, A., Tesic Mark, M., Molina, H., Kohsaka, S., Di Giannatale, A., Ceder, S., Singh, S., Williams, C., Soplop, N., Uryu, K., Pharmer, L., King, T., Bojmar, L., Davies, A. E., Ararso, Y.…Lyden, D. (2015). Tumour exosome integrins determine organotropic metastasis. *Nature*; *527*(7578), 329–335.

Hoshino, A., Kim, H. S., Bojmar, L., Gyan, K. E., Cioffi, M., Hernandez, J., Zambirinis, C. P., Rodrigues, G., Molina, H., Heissel, S., Mark, M. T., Steiner, L., Benito-Martin, A., Lucotti, S., Di Giannatale, A., Offer, K., Nakajima, M., Williams, C., Nogués, L.…Lyden, D. (2020). Extracellular vesicle and particle biomarkers define multiple human cancers. *Cell*; *182*(4), 1044.e18–1061.e18.

Kanada, M., Bachmann, M H., Contag, C H. (2016) Signaling by extracellular vesicles advances cancer hallmarks. *Trends in Cancer*; *2*(2), 84–94.

Karaman, S., & Detmar, M. (2014). Mechanisms of lymphatic metastasis. *Journal of Clinical Investigation*; *124*(3), 922–928.

Lai, C. P., Kim, E. Y., Badr, C. E., Weissleder, R., Mempel, T. R., Tannous, B. A., & Breakefield, X. O. (2015). Visualization and tracking of tumour extracellular vesicle delivery and RNA translation using multiplexed reporters. *Nature Communication*; *6*, 7029.

Liao, Y., Smyth, G. K., Shi, W. (2019) The R package Rsubread is easier, faster, cheaper and better for alignment and quantification of RNA sequencing reads. *Nucleic Acids Research*; *47*(8), e47.

Liu, Y., Gu, Y., Han, Y., Zhang, Q., Jiang, Z., Zhang, X., Huang, Bo, Xu, X., Zheng, J., & Cao, X. (2016). Tumor exosomal RNAs promote lung pre-metastatic niche formation by activating alveolar epithelial TLR3 to recruit neutrophils. *Cancer Cell*; *30*(2), 243–256.

Lobb, R. J., Becker, M., Wen Wen, S., Wong, C. S. F., Wiegmans, A. P., Leimgruber, A., & Möller, A. (2015). Optimized exosome isolation protocol for cell culture supernatant and human plasma. *Journal of Extracellular Vesicles*; *4*, 27031.

Logozzi, M., De Milito, A., Lugini, L., Borghi, M., Calabrò, L., Spada, M., Perdicchio, M., Marino, M. L., Federici, C., Iessi, E., Brambilla, D., Venturi, G., Lozupone, F., Santinami, M., Huber, V., Maio, M., Rivoltini, L., & Fais, S. (2009). High levels of exosomes expressing CD63 and caveolin-1 in plasma of melanoma patients. *Plos One*; *4*(4), e5219.

Love, M. I., Huber, W., & Anders, S. (2014). Moderated estimation of fold change and dispersion for RNA-seq data with DESeq2. *Genome Biology*; *15*(12), 550.

Lu, T. T., & Browning, J. L. (2014). Role of the lymphotoxin/LIGHT system in the development and maintenance of reticular networks and vasculature in lymphoid tissues. *Frontiers in Immunology*; *5*, 47.

Lun, A. T., McCarthy, D. J., & Marioni, J. C. (2016). A step-by-step workflow for low-level analysis of single-cell RNA-seq data with Bioconductor. *F1000Research*; *5*, 2122.

Nathanson, S. D., Shah, R., & Rosso, K. (2015). Sentinel lymph node metastases in cancer: Causes, detection and their role in disease progression. *Seminars in Cell & Developmental Biology*; *38*, 106–116.

Onder, L., Danuser, R., Scandella, E., Firner, S., Chai, Q., Hehlgans, T., Stein, J. V., & Ludewig, B. (2013). Endothelial cell-specific lymphotoxin-beta receptor signaling is critical for lymph node and high endothelial venule formation. *Journal of Experimental Medicine*; *210*(3), 465–473.

Peinado, H., Alečković, M., Lavotshkin, S., Matei, I., Costa-Silva, B., Moreno-Bueno, G., Hergueta-Redondo, M., Williams, C., García-Santos, G., Ghajar, C. M., Nitadori-Hoshino, A., Hoffman, C., Badal, K., Garcia, B. A., Callahan, M. K., Yuan, J., Martins, V. R., Skog, J., Kaplan, R. N....Lyden, D. (2012). Melanoma exosomes educate bone marrow progenitor cells toward a pro-metastatic phenotype through MET. *Nature Medicine*; *18*(6), 883–891.

Peinado, H., Zhang, H., Matei, I. R., Costa-Silva, B., Hoshino, A., Rodrigues, G., Psaila, B., Kaplan, R. N., Bromberg, J. F., Kang, Y., Bissell, M. J., Cox, T. R., Giaccia, A. J., Erler, J. T., Hiratsuka, S., Ghajar, C. M., & Lyden, D. (2017). Pre-metastatic niches: Organ-specific homes for metastases. *Nature Reviews Cancer*.;*17*(5), 302–317.

Phan, T. G., Green, J. A., Gray, E. E., Xu, Y., & Cyster, J. G. (2009). Immune complex relay by subcapsular sinus macrophages and noncognate B cells drives antibody affinity maturation. *Nature Immunology*; *10*(7), 786–793.

Picelli, S., Faridani, O. R., Björklund, Å. K., Winberg, G., Sagasser, S., & Sandberg, R. (2014). Full-length RNA-seq from single cells using Smart-seq2. *Nature Protocols*; *9*(1), 171–181.

Proulx, S. T., Luciani, P., Christiansen, A., Karaman, S., Blum, K. S., Rinderknecht, M., Leroux, J. C., & Detmar, M. (2013). Use of a PEG-conjugated bright near-infrared dye for functional imaging of rerouting of tumor lymphatic drainage after sentinel lymph node metastasis. *Biomaterials*; *34*(21), 5128–5137.

Pucci, F., Garris, C., Lai, C. P., Newton, A., Pfirschke, C., Engblom, C., Alvarez, D., Sprachman, M., Evavold, C., Magnuson, A., Von Andrian, U. H., Glatz, K., Breakefield, X. O., Mempel, T. R., Weissleder, R., & Pittet, M. J. (2016). SCS macrophages suppress melanoma by restricting tumor-derived vesicle-B cell interactions. *Science*; *352*(6282), 242–246.

Ran, F. A., Hsu, P. D., Wright, J., Agarwala, V., Scott, D. A., & Zhang, F. (2013). Genome engineering using the CRISPR-Cas9 system. *Nature Protocols*; *8*(11), 2281–2308.

Schadendorf, D., Gawlik, C., Haney, U., Ostmeier, H., Suter, L., & Czarnetzki, B. M. (1993). Tumour progression and metastatic behaviour in vivo correlates with integrin expression on melanocytic tumours. *Journal of Pathology*. *170*(4), 429–434.

Schadendorf, D., Heidel, J., Gawlik, C., Suter, L., & Czarnetzki, B. M. (1995). Association with clinical outcome of expression of VLA-4 in primary cutaneous malignant melanoma as well as P-selectin and E-selectin on intratumoral vessels. *JNCI: Journal of the National Cancer Institute*; *87*(5), 366–371.

Schindelin, J., Arganda-Carreras, I., Frise, E., Kaynig, V., Longair, M., Pietzsch, T., Preibisch, S., Rueden, C., Saalfeld, S., Schmid, B., Tinevez, J. Y., White, D. J., Hartenstein, V., Eliceiri, K., Tomancak, P., & Cardona, A. (2012). Fiji: An open-source platform for biological-image analysis. *Nature Methods*; *9*(7), 676–682.

Sharma, P., Diergaarde, B., Ferrone, S., Kirkwood, J. M., & Whiteside, T. L. (2020). Melanoma cell-derived exosomes in plasma of melanoma patients suppress functions of immune effector cells. *Science Reports*; *10*(1), 92.

Sheehan, C., & D'souza-Schorey, C. (2019). Tumor-derived extracellular vesicles: Molecular parcels that enable regulation of the immune response in cancer. *Journal of Cell Science*; *132*(20).

Sleeman, J. P. (2015). The lymph node pre-metastatic niche. *Journal of Molecular Medicine (Berl)*; *93*(11), 1173–1184.

Srinivasan, S., Vannberg, F. O., & Dixon, J. B. (2016). Lymphatic transport of exosomes as a rapid route of information dissemination to the lymph node. *Science Reports*; 6, 24436.

Stacker, S. A., Williams, S. P., Karnezis, T., Shayan, R., Fox, S. B., & Achen, M. G. (2014). Lymphangiogenesis and lymphatic vessel remodelling in cancer. *Nature Reviews Cancer*; *14*(3), 159–172.

Stuart, T., Butler, A., Hoffman, P., Hafemeister, C., Papalexi, E., Mauck, W. M., Hao, Y., Stoeckius, M., Smibert, P., & Satija, R. (2019). Comprehensive integration of single-cell data. *Cell*; *177*(7), 1888.e21–1902e21.

Sun, Bo, Zhou, Y., Fang, Y., Li, Z., Gu, X., & Xiang, J. (2019). Colorectal cancer exosomes induce lymphatic network remodeling in lymph nodes. *International Journal of Cancer*; *145*(6), 1648–1659.

Tacconi, C., Commerford, C. D., Dieterich, L. C., Schwager, S., He, Y., Ikenberg, K., Friebel, E., Becher, B., Tugues, S., & Detmar, M. (2021). CD169(+) lymph node macrophages have protective functions in mouse breast cancer metastasis. *Cell Reports*; *35*(2), 108993.

Takeda, A., Hollmén, M., Dermadi, D., Pan, J., Brulois, K. F., Kaukonen, R., Lönnberg, T., Boström, P., Koskivuo, I., Irjala, H., Miyasaka, M., Salmi, M., Butcher, E. C., & Jalkanen, S. (2019). Single-cell survey of human lymphatics unveils marked endothelial cell heterogeneity and mechanisms of homing for neutrophils. *Immunity*; *51*(3), 561.e5–572.e5.

Tamburini, B. A., Burchill, M. A., & Kedl, R. M. (2014). Antigen capture and archiving by lymphatic endothelial cells following vaccination or viral infection. *Nature Communication*; *5*, 3989.

Tewalt, E. F., Cohen, J. N., Rouhani, S. J., Guidi, C. J., Qiao, H., Fahl, S. P., Conaway, M. R., Bender, T. P., Tung, K. S., Vella, A. T., Adler, A. J., Chen, L., & Engelhard, V. H. (2012). Lymphatic endothelial cells induce tolerance via PD-L1 and lack of costimulation leading to high-level PD-1 expression on CD8 T cells. *Blood*; *120*(24), 4772–4782.

Théry, C., Witwer, K. W., Aikawa, E., Alcaraz, M. J., Anderson, J. D., Andriantsitohaina, R., Antoniou, A., Arab, T., Archer, F., Atkin-Smith, G. K., Ayre, D. C., Bach, J. -M., Bachurski, D., Baharvand, H., Balaj, L., Baldacchino, S., Bauer, N. N., Baxter, A. A., Bebawy, M....Zuba-Surma, E. K. (2018). Minimal information for studies of extracellular vesicles 2018 (MISEV2018): A position statement of the International Society for Extracellular Vesicles and update of the MISEV2014 guidelines. *Journal of Extracellular Vesicles*; *7*(1), 1535750.

Tkach, M., & Théry, C. (2016). Communication by extracellular vesicles: Where we are and where we need to go. *Cell*; *164*(6), 1226–1232.

Witwer, K. W., & Théry, C. (2019). Extracellular vesicles or exosomes? On primacy, precision, and popularity influencing a choice of nomenclature. *Journal of Extracellular Vesicles*; *8*(1), 1648167.

Zhu, M., & Fu, Y. X. (2011). The role of core TNF/LIGHT family members in lymph node homeostasis and remodeling. *Immunological Reviews*; *244*(1), 75–84.

SUPPORTING INFORMATION

Additional supporting information may be found in the online version of the article at the publisher's website.